

Imaging the effect of a non-magnetic impurity in a RVB superconductor

Manuela Capello¹ and Didier Poilblanc^{2,1}

¹Laboratoire de Physique Théorique, CNRS and Université de Toulouse, F-31062 Toulouse, France

²Institute of Theoretical Physics, Ecole Polytechnique Fédérale de Lausanne, CH-1015 Lausanne, Switzerland

(Dated: December 10, 2018)

The effects of an individual non-magnetic impurity in a high-temperature gapless superconductor is analyzed within the t-J model by Variational Monte Carlo simulations of fully-optimized Resonating Valence Bond wavefunctions. The spatial dependance of the hole density and of the valence bond and superconducting pairing amplitudes show a cross-shaped four-fold symmetric structure similar to the observed scanning tunneling microscopy measurements in a lightly Zinc-substituted cuprate superconductor.

Introduction – Cuprates superconductors can be considered as doped two-dimensional (2D) Mott insulators where electronic correlations play a dominant role^{1,2}. A number of exotic properties such as the pseudo-gap behavior reflect the complexity of the system. In a pioneering work, Anderson proposed the Resonating Valence Bond (RVB) Mott insulator as the relevant underlying parent state³ from which gapless d-wave superconductivity naturally emerges under doping. A mean-field version of the RVB theory⁴ provides an appealing physical origin of the pseudo-gap as the energy scale associated to the formation of singlet electron pairs via the nearest-neighbor antiferromagnetic (AF) exchange.

Local probes of correlated materials with atomic resolution have recently become possible thanks to Scanning Tunneling Microscopy (STM)⁵ which provided unprecedented high-resolution maps of the surface of some underdoped cuprate superconductors⁶. The measured space-resolved doped-hole charge density in the SC regime of Na-CCOC and Dy-Bi2212 cuprates revealed stripe patterns⁷. This discovery naturally raises the question whether such inhomogeneities are induced by impurities or whether they are intrinsic as the bulk static charge and spin stripe orders detected in Nd-LSCO⁸ and LBCO⁹ cuprates at doping $\delta \sim 1/8$.

Substituting a single impurity atom for a copper atom indeed strongly affects its surrounding region. Reversely, it can serve as a very useful local probe, providing important insights about the properties of the correlated medium itself¹⁰. In fact, imaging the effect of individual zinc impurity atoms on superconducting Bi2212 has been performed by STM¹¹ showing clear real-space modulations which can be confronted to theoretical modeling. Our aim here is to compare these experimental STM observations to a simple model for a zinc impurity in a copper-oxide superconducting plane using a t-J model description for the bulk¹.

The $t - J$ Hamiltonian on a square lattice reads,

$$H_{t-J} = - \sum_{\langle i,j \rangle \sigma} t_{ij} (c_{i\sigma}^\dagger c_{j\sigma} + h.c.) + \sum_{\langle i,j \rangle} J_{ij} S_i \cdot S_j. \quad (1)$$

A zinc impurity is in the same 2+ oxidation state as the copper ion it is substituted for, so that it does not introduce extra charge. However, in contrast to the copper

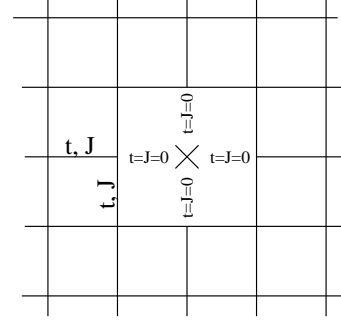


FIG. 1: Schematic representation of the impurity model. The cross corresponds to the impurity site i_0 . The parameters t and J are set to zero on the four bonds connected to the impurity site.

$S=1/2$ ion, the Zn^{2+} ion is in a spin-singlet state, inert magnetically. Hence, one can use a simple description : on the four bonds connected to the impurity site we set $t_{ij} = 0$ and $J_{ij} = 0$ as shown on Fig. 1. On all the other bonds, we set t_{ij} and J_{ij} to the same values t and J , respectively. Although completely local such a "boundary" is expected to lead to a *spatially* extended perturbation affecting GS properties.

Description of method – Our aim is now to built variational RVB wave-functions (WFs) for the t-J model on finite $L \times L$ clusters with periodic-boundary conditions and containing a single impurity. In practice we shall consider $L = 8$ and $L = 16$. A Variational Monte Carlo (VMC) scheme¹² is used to (i) realize a thorough optimization over the (numerous) variational parameters¹³ and (ii) to calculate accurately the ground-state (GS) energies and physical observables. The presence of the impurity on site i_0 modifies the Hilbert space, i.e. $c_{i_0\sigma}^\dagger |\Psi\rangle = 0$ and $c_{i_0\sigma} |\Psi\rangle = 0$, where $|\Psi\rangle$ is the GS of the system. In our Monte Carlo variational scheme an "impurity projector" $\mathcal{P}_{i_0} = (1 - n_{i_0\uparrow})(1 - n_{i_0\downarrow})$ is inserted, and the impurity variational wavefunction is defined as:

$$|\Psi_{\text{VMC}}\rangle = \mathcal{P}_g \mathcal{P}_{i_0} |D\rangle, \quad (2)$$

where \mathcal{P}_g is the usual Gutzwiller projector enforcing the constraint of no-double occupancy on the remaining $L^2 - 1$ sites.

A fair and accurate description of the system relies then crucially on the choice of the above mean-field determinant $|D\rangle$. The later can be of two types; (i) It can be the ground-state $|D(L \times L)\rangle$ of a mean-field Hamiltonian defined on *all* of the 8×8 sites. The orbitals are defined on i_0 , and the site i_0 is always occupied by a hole; (ii) It can be the ground-state $|D(L \times L - 1)\rangle$ of a mean-field Hamiltonian defined only on the $L^2 - 1$ sites excluding the impurity site i_0 ¹⁴. The mean field Hamiltonian we consider to construct $|D\rangle$ is of standard BCS-type:

$$H_{\text{MF}} = \sum_{\langle i,j \rangle \sigma} (\chi_{ij} c_{i\sigma}^\dagger c_{j\sigma} + h.c.) + \sum_{\langle i,j \rangle} (\Delta_{ij} c_{i\uparrow}^\dagger c_{j\downarrow}^\dagger + h.c.) + \mu \sum_{i\sigma} n_{i\sigma} \quad (3)$$

where we optimize *all* different non-equivalent bonds around the impurity, starting from an initial guess respecting or not the square lattice symmetry around i_0 . Since in principle the Hamiltonian C_{4v} symmetry around i_0 (see Figure 1) could be spontaneously broken, we have performed a number of preliminary tests on small 8×8 lattices, choosing the initial RVB bonds pattern with lower symmetries like e.g. C_4 or C_{2v} symmetries (the later allowing the formation of a domain wall). We have found that the full C_{4v} symmetry is systematically restored at the variational minimum. Therefore, to reduce the number of variational parameters and gain accuracy on our largest 16×16 cluster, we have enforced from the start the C_{4v} symmetry. Also we have found that optimizing different μ_i is not essential to gain energy so that a uniform chemical potential can be assumed.

Before moving to 16×16 clusters, a series of other tests have been performed on the smaller 8×8 lattice at $\delta = 1/8$ with different choices of determinants:

- (I) Optimize $|D(8 \times 8 - 1)\rangle$ with all possible Δ_{ij} connecting the $L^2 - 1$ sites ($\chi_{ij} = 1$ everywhere).
- (II) Optimize $|D(8 \times 8)\rangle$ with all possible Δ_{ij} but fix $\Delta_{ij} = \chi_{ij} = 0$ on the four $t = J = 0$ bonds (and $\mu_{i_0} = 0$).
- (III) Optimize $|D(8 \times 8)\rangle$ with all possible Δ_{ij} and χ_{ij} (including the impurity bonds).

As expected, all optimized WFs are found to show locally opposite signs of Δ_{ij} on any site-sharing vertical and horizontal bonds, hence reflecting the expected *orbital d-wave character* of the superconducting order. The lowest-energy state (III) is obtained for a full optimization of the Δ_{ij} and χ_{ij} parameters over *all* bonds. Note that, although $\Delta_{ij} \simeq 0$, χ_{ij} has a significant magnitude on the four bonds connected to the impurity site. Moreover, for smaller doping (see the 16×16 calculations), a large magnitude of Δ_{ij} also appears on the later bonds. Note that the $|D(8 \times 8 - 1)\rangle$ determinant (I) has a much higher energy. In the following we report results for the best variational wavefunction (case III) on 16×16 clusters and $t/J = 3$.

TABLE I: Variational energy per site (in units of t) for different projected WFs for the $t-J$ model at doping $1/8$ ($N_h = 8$), for $t/J = 3$ and a 8×8 cluster with an impurity.

$ D\rangle$	$E_{\text{VMC}}[t]$
(I)	-0.41477(5)
(II)	-0.41930(5)
(III)	-0.41968(5)

Results on 16×16 clusters – We now turn to the VMC calculations on the 16×16 cluster with periodic-boundary conditions. Here, we consider a physical "core" 8×8 region centered around the impurity (i.e. of the same size as our previous small cluster), where we impose a C_{4v} symmetry around the impurity site. Outside, we assume a uniform d-wave superconducting background (bg) whose parameters $\chi_{i,i+\hat{x}} = \chi_{i,i+\hat{y}} = \chi_{\text{bg}}$ and $\Delta_{i,i+\hat{x}} = -\Delta_{i,i+\hat{y}} = \Delta_{\text{bg}}$ are optimized simultaneously. This enables to reduce significantly the boundary effects and is justified since the spatial extension of the effect of the impurity rarely exceeds the assumed size of the core.

The spacial distribution of the local hole density $\langle c_{i\sigma} c_{i\sigma}^\dagger \rangle$, the bond hole kinetic amplitudes $K_{ij} = \langle (c_{j\sigma} c_{i\sigma}^\dagger + h.c.) \rangle$ and the magnetic VB amplitudes $S_{ij} = \langle \mathbf{S}_i \cdot \mathbf{S}_j \rangle$ are shown in Fig. 2(a) and in Fig. 3(a), respectively, for doping $1/8$. Here, and throughout the paper, we only show the 6×6 central region exhibiting the largest modulations. It turns out that the variational parameters Δ_{ij} are suppressed on the four bonds connected to the impurity. This is compensated by an increase in Δ_{ij} and hence of S_{ij} on the neighboring bonds, forming a cross-like structure (see thick blue bonds of Fig. 3(a)). Due to similarities with work done in a somewhat different context¹⁶, we shall refer to these bonds as the four "dimer bonds". These bonds are characterized by a simultaneous hole deficiency and a large gain in the magnetic energy (which can reach more than 40%), hence signaling a tendency towards singlet crystallization around the impurity. The distribution of K_{ij} in Fig. 2 shows also a remarkably strong modulation around the impurity.

Superconducting properties of RVB states are characterized by the singlet-pair correlations at distance \mathbf{r} , $\langle \Psi_{\text{VMC}} | \tilde{\Delta}_{\mathbf{s}+\mathbf{r}}^\dagger \tilde{\Delta}_{\mathbf{s}} | \Psi_{\text{VMC}} \rangle / \langle \Psi_{\text{VMC}} | \Psi_{\text{VMC}} \rangle$, where the operator $\tilde{\Delta}_{\mathbf{s}}^\dagger = c_{i(\mathbf{s}),\uparrow}^\dagger c_{j(\mathbf{s}+\hat{\mathbf{a}}),\downarrow}^\dagger - c_{i(\mathbf{s}),\downarrow}^\dagger c_{j(\mathbf{s}+\hat{\mathbf{a}}),\uparrow}^\dagger$ creates a singlet pair of electrons on the bond between locations \mathbf{s} and $\mathbf{s} + \hat{\mathbf{a}}$ on the lattice, $\hat{\mathbf{a}}$ being the unit vector that specifies the bond direction (along x or y). On the 8×8 cluster, we have computed pairing correlations between separate bonds for increasing bond separation. However, at the largest distance available on this cluster, the correlations have not completely reached saturation. To get a better estimation of the superconducting order parameter we have considered the 16×16 cluster and computed the pairing amplitudes $\tilde{\Delta}_{ij}$ for all bonds (i, j) within the

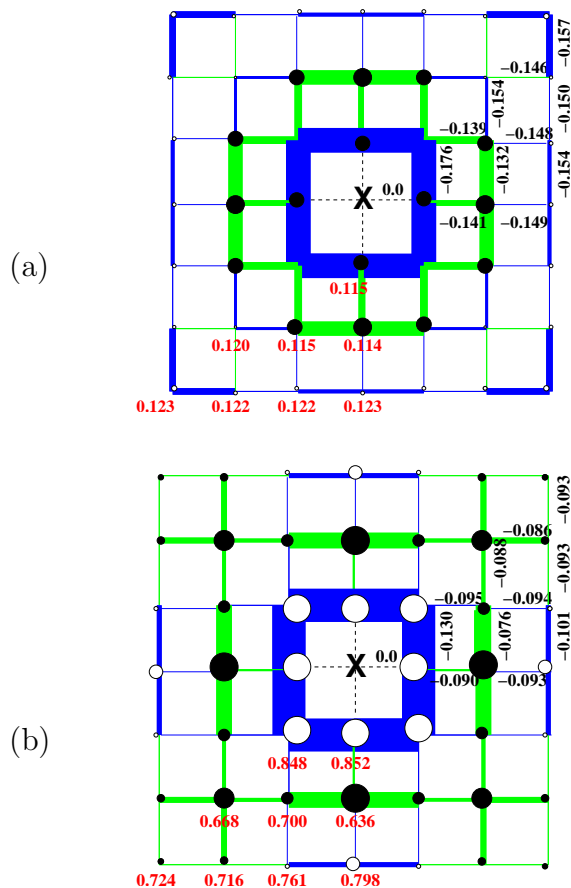


FIG. 2: (Color online.) VMC results for the GS on-site hole densities (circles) and kinetic bond amplitudes (colored segments) obtained on a 16×16 cluster. Only the central region around the impurity is shown. Diameters of circles and widths of segments scale with the *absolute value* of the *relative* differences w.r.t. the impurity-free homogenous state at the same δ_{ave} hole density (whose reference values are estimated by interpolating pure clusters with available flanking hole densities). Higher (lower) hole densities and bond magnitudes w.r.t. the homogeneous case are shown by open (filled) circles and blue (green) bonds respectively. For completeness, we also show on the plot the (bare) numerical values of the non-equivalent sites/bonds. (a) and (b) corresponds to 32 ($\delta_{\text{ave}} \simeq 0.1255$) and 20 ($\delta_{\text{ave}} \simeq 0.0784$) doped holes giving rise, for an homogeneous background, to $E_{\text{kin}}^{\text{homog}}/t = -0.1487$ and $E_{\text{kin}}^{\text{homog}}/t = -0.0941$ per bond, respectively.

”core” region,

$$\bar{\Delta}_{i(s),j(s+\hat{\mathbf{a}})} = \frac{\langle \tilde{\Delta}_{\mathbf{s}} \tilde{\Delta}_{\mathbf{bg}} \rangle}{\sqrt{\langle \tilde{\Delta}_{\mathbf{bg}} \tilde{\Delta}_{\mathbf{bg}} \rangle}}, \quad (4)$$

where $\tilde{\Delta}_{\mathbf{bg}}$ is a pair operator on the most remote bond in the homogeneous background. As shown in Fig. 4(a), pairing is enhanced on the dimer bonds, and is depleted around the impurity, where holes are less present.

The 16×16 cluster also allows to reduce the doping content, e.g. to 20 holes, going further into the under-

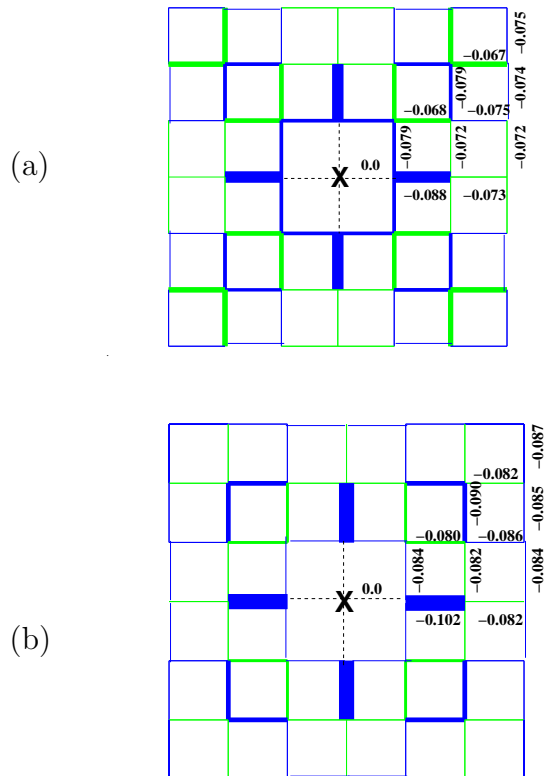


FIG. 3: (Color online.) VMC results for the GS magnetic bond amplitudes obtained on a 16×16 cluster. Same conventions and parameters as in Fig.2. (a) and (b) corresponds to 32 ($\delta_{\text{ave}} \simeq 0.1255$) and 20 ($\delta_{\text{ave}} \simeq 0.0784$) doped holes giving rise for an homogeneous background to $E_{\text{mag}}^{\text{homog}}/J = -0.074$ and $E_{\text{mag}}^{\text{homog}}/J = -0.084$ per bond, respectively.

doped region. Interestingly, the hole distribution around the defect is very sensitive to the doping ratio. Indeed, for doping around 12.5% (32 holes) we found that holes are slightly repelled from the bonds around the impurity. In contrast, for 7.8% doping, holes tend to concentrate more around the impurity site as shown in Fig. 2(b). The variational pairing Δ_{ij} becomes stronger on the impurity bonds suggesting the formation of a ”hole pair” with the impurity *empty* site. The corresponding real space modulations of S_{ij} and $\bar{\Delta}_{ij}$ are shown in Figs. 3(b) and 4(b).

Discussions – Let us now compare our findings to prior theoretical approaches. The first investigation of a single impurity immersed in a correlated host has been performed using Lanczos exact diagonalization of small clusters. A calculation of the local density of states¹⁷ revealed bound-states (of different orbital symmetries) in which a mobile hole is trapped by the induced impurity potential. Here, a unique mobile hole was assumed in the cluster, hence preventing real bulk pairing and giving rise to a very small doping $\sim 5\%$ in the surrounding region. Although our VMC calculations are done in a different physical range (and on much larger clusters), we find, for

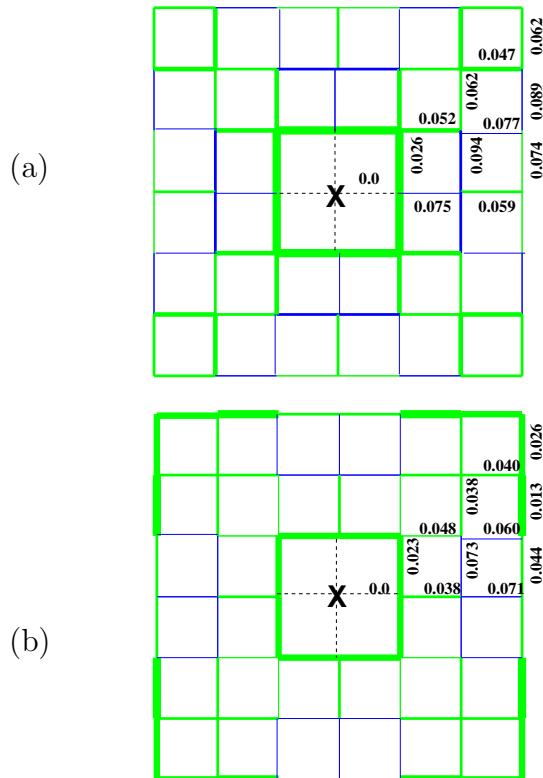


FIG. 4: (Color online.) VMC results for the pairing bond amplitudes $\bar{\Delta}_{ij}$ obtained on a 16×16 cluster. Same conventions and parameters as in Fig.2. (a) and (b) corresponds to 32 ($\delta_{\text{ave}} \simeq 0.1255$) and 20 ($\delta_{\text{ave}} \simeq 0.0784$) doped holes giving rise, for an homogeneous background, to $\Delta_{\text{bg}} \simeq 0.0787$ and $\Delta_{\text{bg}} \simeq 0.0626$, respectively.

decreasing doping, the emergence of excess hole density around the impurity, which possibly could be consistent

with a bound-state formation when $\delta \rightarrow 0$.

Metlitski and Sachdev¹⁵ have introduced a theory of valence bond solid (VBS) correlations near a single impurity in a square lattice antiferromagnet. When the system is close to a quantum transition from a magnetically ordered Néel state to a spin-gap state with long-range VBS order, a missing spin gives rise to a VBS pinwheel (or "vortex") around the impurity¹⁶. To compare with these predictions we have computed the VBS order parameter of Eq.(5) in Ref. 16. However, despite many similarities (e.g. crystallization of dimer bonds in the vicinity of the impurity), the vortex structure is not recognizable in our simulation. We hypothesize that (i) our system is probably not close enough to the critical point assumed in Ref. 15,16 and/or (ii) the VBS region develops differently in a d-wave RVB than in an AF background.

Lastly, our results are compared to the experimental STM observations around a Zn impurity in a Bi2212 cuprate superconductor shown in Ref. 11. First, we point out that GS properties have been calculated here while Ref. 11 reports spectral properties. However, since equal-time and frequency-dependent quantities are related via a simple frequency integration up to a physical cutoff (see e.g. Ref. 7 for derivation of the local hole-charge distribution from space-resolved tunneling spectra) both sets of data should reveal similarities. Indeed, like in the experiments, the patterns we found show clearly a cross-shaped symmetric structure suggesting that the theoretical modeling of the impurity associated to a RVB description of the superconductor are realistic.

Acknowledgments

We acknowledge support from the French Research Council (ANR). D.P. also thanks S. Sachdev for insightful discussions.

¹ F. C. Zhang and T. M. Rice, Phys. Rev. B **37**, 3759 (1988).
² S. Sachdev, Rev. Mod. Phys. **75**, 913 (2003).
³ P. W. Anderson, Science **235**, 1196 (1987).
⁴ F. C. Zhang, C. Gros, T.M. Rice and H. Shiba, Supercond. Sci. Technol. **1**, 36 (1988).
⁵ O. Fischer, M. Kugler, I. Maggio-Aprile, C. Berthod and C. Renner, Rev. Mod. Phys. **79**, 353 (2007).
⁶ T. Valla, A.V. Fedorov, Jinho Lee, J.C. Davis and G.D. Gu, Science **314**, 1914 (2006).
⁷ Y. Kohsaka *et al.*, Science **315**, 1380 (2007); see also J. Zaanen, *ibid.* **315**, 1372 (2007).
⁸ J. M. Tranquada *et al.*, Nature (London) **375**, 561 (1995); N. B. Christensen *et al.*, Phys. Rev. Lett. **98**, 197003 (2007).
⁹ P. Abbamonte *et al.*, Nature Physics **1**, 155 (2005); J.M. Tranquada *et al.*, Phys. Rev. B **78**, 174529 (2008).
¹⁰ M. I. Salkola, A. V. Balatsky, and D. J. Scalapino, Phys. Rev. Lett. **77**, 1841 (1996).

¹¹ S.H. Pan, E.W. Hudson, K.M. Lang, H. Eisaki, S. Uchida and J.C. Davis, Nature **403**, 746 (2000).
¹² C. Gros, Phys. Rev. B **38**, 931 (1988); S. Sorella *et al.*, Phys. Rev. Lett. **88**, 117002 (2002).
¹³ VMC has been recently extended to handle non-uniform states; see M. Capello, M. Raczkowski and D. Poilblanc, Phys. Rev. B **77**, 224502 (2008).
¹⁴ Strictly speaking, for N_h mobile holes in the cluster, the average doping of the surrounding medium is $\delta_{\text{ave}} = N_h/(L^2 - 1)$, higher than the nominal doping $\delta = N_h/L^2$.
¹⁵ M.A. Metlitski and S. Sachdev, Phys. Rev. B **77**, 054411 (2008).
¹⁶ R.K. Kaul, R.G. Melko, M.A. Metlitski and S. Sachdev, Phys. Rev. Lett. **101**, 187206 (2008); M.A. Metlitski and S. Sachdev, Phys. Rev. B **78**, 174410 (2008).
¹⁷ D. Poilblanc, D. J. Scalapino, and W. Hanke, Phys. Rev. Lett. **72**, 884 (1994).